Environmentally friendly synthesis and characterization of copper nanoparticles using amino acids as capping agents: enhanced corrosion resistance and morphological control

N. Muneam,[1] F.F. Sayyid,[1] M.H.H. Al-Kaabi[2] and A.A. Alamiery[3,4]*

[1]*Department of Production Engineering and Metallurgical, University of Technology, Baghdad, 10001, Iraq*
[2]*Basrah University for Oil and Gas, Basrah, 61004, Iraq*
[3]*University of Technology, Baghdad, 10001, Iraq*
[4]*University Kebangsaan Malaysia, Bangi 43000, Selangor, Malaysia*
**E-mail: dr.ahmed975@gmail.com*

Abstract

This research presents the synthesis and characterization of copper nanoparticles employing amino acids, specifically *L*-arginine and *L*-aspartic acid, as capping agents at varying concentrations (0.25, 0.50, 0.75 and 1 g). The study aims to modify corrosion resistance, crystal size, and surface morphology through electrodeposition using a solution containing $CuSO_4$ and additives. Prior to the addition of amino acids, the influences of copper concentration and H_2SO_4 concentration on the apparent density, shape, and particle size of the resulting powder were investigated. Characterization techniques, including XRD pattern analysis, FE-SEM scanning electron microscopy, dynamic light scattering (DLS), zeta potential, and FTIR, were employed. The scanning electron microscopy images revealed well-distributed particles with an average size of approximately 30 nm. Additionally, the research explores the impact of camel saliva as an additive on the morphology and particle size of copper powder during the electrodeposition process. The overarching objective is to identify non-toxic and environmentally friendly leveling agents, with a focus on utilizing amino acids for an in-depth investigation into the copper dissolution reaction. This understanding contributes to elucidating the redox reactions involved when metals dissolve in strong acids, providing insights into the development of inhibitory materials that yield nanoscale sizes. Such nanomaterials find applications in diverse fields, including medicine, electronics, and industry.

Received: December 16, 2023 Published: February 10, 2024 doi: 10.17675/2305-6894-2024-13-1-14

Keywords: *corrosion, saliva, electrodeposition, copper, sulphate.*

1. Introduction

Corrosion is a natural process that occurs when metals, such as copper, react with their environment, leading to the deterioration of the metal's properties [1–8]. Copper, despite its commendable conductivity and versatility, is not immune to the effects of corrosion. The corrosion of copper primarily involves the formation of copper oxide layers on the metal

surface due to its interaction with oxygen and moisture in the environment. This process is often accelerated in the presence of corrosive agents like acids or salts [9–12]. Copper corrosion typically begins with the oxidation of the metal. When exposed to atmospheric oxygen, copper undergoes a series of reactions, forming copper oxide (Cu_2O) or copper hydroxide ($Cu(OH)_2$) layers on its surface [13–15]. These oxide layers, commonly known as patina, can have varying colors and compositions, ranging from brown to green. The corrosion products that develop on copper surfaces act as protective layers to some extent [16–18]. However, in certain environments, these layers may not be sufficiently protective, leading to further corrosion. Additionally, the presence of pollutants or aggressive chemicals can accelerate the corrosion process, compromising the integrity of copper components [19–21]. Pitting corrosion is a specific form of corrosion that can affect copper. It involves the localized degradation of the metal surface, resulting in the formation of small pits. Pitting corrosion can significantly reduce the strength and durability of copper, making it susceptible to structural failure. When copper comes into contact with dissimilar metals in the presence of an electrolyte, galvanic corrosion can occur. This electrochemical process leads to the accelerated corrosion of the less noble metal, which, in the case of copper, can be exacerbated when coupled with metals like iron or aluminum. In practical terms, the corrosion of copper is of particular concern in various applications, including plumbing, electrical wiring, and industrial equipment. Corrosion-induced degradation can compromise the efficiency and safety of these systems, necessitating preventive measures and materials modifications [22–25]. Understanding the mechanisms and factors influencing copper corrosion is crucial for developing strategies to mitigate its impact. Researchers often explore innovative approaches, such as the use of additives and protective coatings, to enhance copper's corrosion resistance and extend its functional lifespan in diverse applications [26, 27]. The aforementioned research on copper nanoparticles using amino acids as capping agents represents one such effort to tailor copper properties and combat corrosion through advanced materials synthesis.

The synthesis of nanoparticles with tailored compositions, sizes, and shapes is pivotal for unlocking their potential applications in catalysis, sensors, microelectronics, and various realms of nanotechnology [29]. Metal nanoparticles (NPs) have recently garnered considerable interest owing to their distinct physicochemical properties, which can be modulated based on the synthesis process. The antimicrobial efficacy of nanoparticles is notably influenced by the control of particle size [30]. At the nanoscale, materials undergo abrupt changes in optical, thermal, and electromagnetic properties, leading to small-scale, surface-level, and quantum-scale effects. Copper nanoparticles, distinguished by cost-effectiveness and specific surface area advantages, have emerged as a focal point for researchers. Electrodeposition, a top-down synthesis method, offers a cost-effective approach to fabricating high-quality CuNPs, with their attributes contingent on deduction methods and electrochemical process parameters. This research endeavors to deduce the mean size of CuNPs [31, 32]. In the pursuit of environmentally friendly and non-harmful materials, biological agents have been introduced to form complexes with inorganic

materials, facilitating diffusion without agglomeration. Despite advancements, synthesizing well-dispersed copper particles using eco-friendly materials remains challenging. Amino acids, crucial as covering and reducing agents for metals, present a promising avenue for nanoparticle synthesis. Notably, the amino acids found in the saliva of one-humped camels from southern Iraq exhibit chelating properties, forming highly stable complexes capable of enveloping metal ions [33]. Nanoparticles serve as fundamental building blocks in nanotechnology, serving as the cornerstone for the production of nanostructured materials and tools. The production of nanoparticles plays a pivotal role in advancing research in nanoengineering and nanoscience. Diverse types of nanoparticles are prepared using raw materials in solid, liquid, and gaseous phases, aligning nanostructures through chemical reactions or physical pressure [34]. The objectives of the research are:

- To synthesize copper nanoparticles using amino acids (*L*-Arginine and *L*-Aspartic acid) as capping agents in varying concentrations.
- To investigate the impact of copper concentration and H_2SO_4 concentration on the apparent density, shape, and particle size of synthesized copper nanoparticles;
- To analyze the influence of camel saliva, as an additive, on the morphology and particle size of copper powder during the electrodeposition process.
- To characterize the synthesized nanoparticles using XRD, FE-SEM, DLS, zeta potential, and FTIR techniques.
- To contribute to the understanding of redox reactions occurring during the dissolution of metals in strong acids, focusing on inhibitory materials for various applications in medical, electronic, and industrial fields.

2. Role of Amino Acids in Electrodeposition

Amino acid-based additives have emerged as effective agents for tailoring various aspects of electrodeposition processes, including corrosion resistance, crystal size, surface morphology, and deposit adhesion. Some specific amino acids have shown promise in enhancing copper electrodeposition from acid baths [35, 36]. The electrodeposition technique offers notable advantages such as time efficiency, cost-effectiveness, high deposition rates, and the use of relatively inexpensive equipment owing to the absence of vacuum technology [37–39]. The convergence of nanobiotechnology and electrodeposition, leveraging the unique properties of amino acids, represents a novel and globally intriguing concept within the realm of nanotechnology [40]. Chelated minerals, formed by the complexation of metals with amino acids, offer advantages such as the use of small quantities, cost-effectiveness, and high repayment rates. The resulting metal-chelated amino acid complexes exhibit specific properties distinct from metal sulfate salts, with these properties being contingent on the metal ion and ligand type [41, 42]. In the coordination chemistry of transition metals, which is integral to this process, coordinate covalent bonds are formed. This Lewis acid-base interaction involves a central metal ion, often a transition or internal transition metal, forming bonds with ligands–atoms, molecules, or ions–with one or more

pairs of electrons available for donation. The coordination domain encompasses the central metal ion and its associated ligands [43–45].

Among the commercially valuable copper (II) compounds, cupric oxide (CuO), cupric chloride ($CuCl_2$), and cupric sulfate ($CuSO_4$) play significant roles. Cupric oxide, existing as a black powder and found in minerals like tenorite and paramelaconite (Figure 1) [13], holds particular relevance in this context. The introduction of a diverse range of ligands has the potential to enhance our understanding of particle-ligand interactions, presenting new avenues to modulate performance. Ligands, covalently coordinated to the metal nanoparticle surface, can be categorized as anionic (X-type), neutral (L-type), or cationic (Z-type) based on their donor atoms. This classification aligns with the covalent bond classification (CBC) theory [46–50].

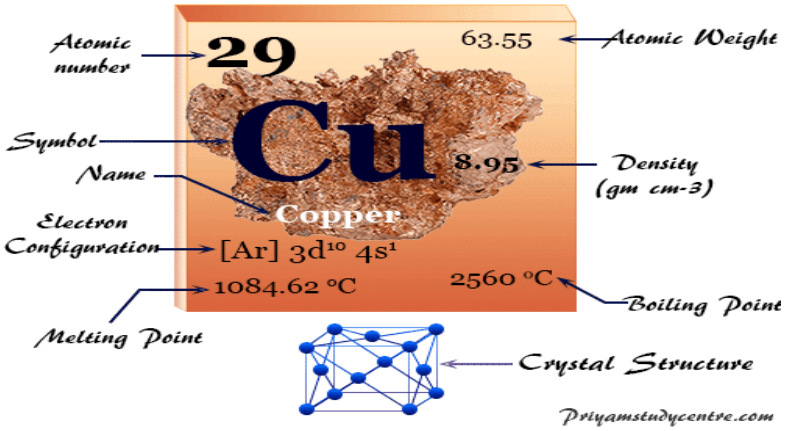

Figure 1. Metal forming a face-centered cubic crystal lattice.

3. Experimental Details

The experimental methods employed in this study encompassed various techniques and conditions. Detailed information on the equipment, procedures, and parameters is provided below:

- Scanning electron microscope (SEM): SEM imaging was conducted using the JEOL Ltd. JSM-7100F scanning electron microscope, located in Tokyo, Japan. The instrument was employed to study the surface morphology of copper powder.
- Energy dispersive analysis: energy dispersive analysis was performed as part of the SEM analysis to obtain information on the elemental composition of the samples. The SEM-EDS system was utilized for this purpose.
- Infrared (IR) spectra: IR spectra were recorded using BRUKER, Germany, scanner with such a scanning range from 450–4000 cm^{-1}. The Infrared (IR) spectra analysis was conducted to assess the chemical composition and molecular structure of the synthesized copper nanoparticles. The following procedure outlines the steps taken during the IR spectroscopy experiment:

1. Sample preparation: copper nanoparticles obtained from the electrodeposition process were prepared for IR analysis. The samples were carefully collected and ground into a fine powder to ensure uniformity.
2. Instrumentation: an infrared spectrophotometer was employed for the analysis. The instrument was equipped with a high-quality IR source, interferometer, and detector for accurate measurements.
3. Sample presentation: the finely powdered copper nanoparticles were placed onto a suitable sample holder. The sample holder material was chosen to be transparent in the IR region to minimize interference.
4. Baseline measurement: prior to sample analysis, a baseline spectrum of the empty sample holder or a reference material was recorded. This served as a reference for subtracting background signals.
5. IR Spectra collection: the sample was exposed to infrared radiation over a specific wavelength range. The instrument recorded the absorption of infrared light by the sample at different frequencies, generating an IR spectrum.
6. Data analysis: the obtained IR spectrum was analyzed for characteristic absorption peaks corresponding to functional groups present in the copper nanoparticles. Peaks were identified based on known vibrational frequencies of chemical bonds.
7. Interpretation: interpretation of the IR spectra involved correlating observed peaks with molecular vibrations of amino acids from the camel saliva and other potential compounds in the synthesized copper nanoparticles.
8. Documentation: the final IR spectra, along with peak assignments and interpretations, were documented. Any notable shifts or new peaks were reported as indicators of chemical interactions or modifications in the synthesized nanoparticles.
9. Polarization studies: polarization studies were conducted to investigate corrosion behavior. The experiments involved working electrodes (316 stainless steel), an anode electrode (copper alloy), and a solution containing hydrated copper sulfate salt ($CuSO_4 \cdot 5H_2O$) and fresh camel saliva (amino acids). The solution comprised hydrated copper sulfate salt and fresh camel saliva.

The electrolysis process is comprised of three essential components:

1. External circuit: this includes a power supply as a direct current (DC) source, instruments like ammeters, voltmeters, and regulators to maintain desired values, and a pH meter for acidity measurement during the process (Figure 2).
2. Electrodes: the working electrodes or cathodes (316 stainless steel) measure 2.8 cm×10 cm×2 mm, while the anode electrode, prepared from a copper alloy (97.200%), measures 8 cm×3 cm×3 mm. Chemical analyses of both cathode and anode plates are presented in Table 1.
3. Solution container: a heat-resistant glass flask holds the solution consisting of hydrated copper sulfate salt ($CuSO_4 \cdot 5H_2O$) with fresh camel saliva (amino acids)

as an additive. Continuous mixing using a magnetic mixer ensures solution homogeneity under operational conditions.

Table 1. Chemical composition.

Element	Fe	V	Cr	Ni	Mo	Mn	Mg	Al	Si
Cathode	64.79	0.0787	17.16	11.79	1.423	1.613	0.419	0.595	0.7
Element	Cu	Al	Si	Mg	P	S	Ti	V	–
Anode	97.20	0.945	0.297	0.310	0.022	0.0134	0.0299	0.0196	

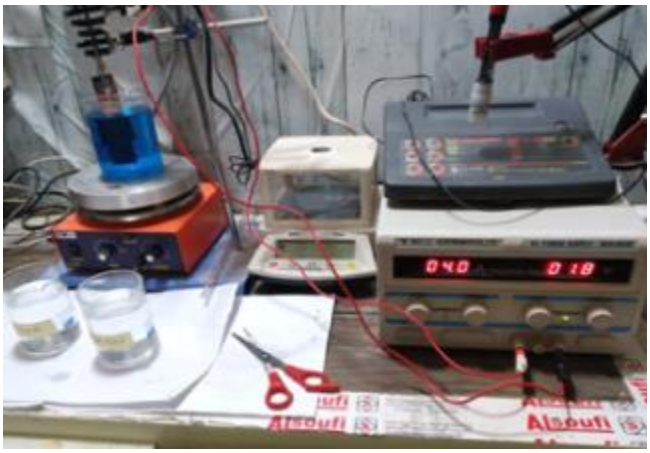

Figure 2. Electrodeposition cell.

3.1. Effect of copper sulfate concentration

3.1.1. Effect of copper ion concentration

The study investigates the reaction mechanisms at five different copper concentrations (40, 60, 80, 100 and 120 g/l). Table 2 outlines the operating conditions for varying copper sulfate concentrations.

Table 2. Operating conditions for varying copper sulfate concentration.

$CuSO_4$ (g/l)	H_2SO_4 (ml/l)	Current (A)	Potential (V)	pH	Time (min)	Electrical conductivity (mS/m)	Copper powder (g)
40	50	3.0	2.5–3.9	0.34–1.43	60	12.34	2.21
60	50	3.0	2.6–3.8	0.52–1.38	60	27.2	2.01
80	50	3.0	2.4–4.0	0.47–1.26	60	33.7	3.13
100	50	3.0	2.3–3.9	0.32–0.91	60	35.6	1.82
120	50	3.0	2.4–3.8	0.21–0.82	60	38.4	1.74

Conclusions from Table 2:

- The study investigated the reaction mechanisms at different copper concentrations, ranging from 40 g/l to 120 g/l.
- Operating conditions, including current, potential, pH, and time, were consistent across the experiments.
- The electrical conductivity increased with higher copper concentrations, reaching a maximum of 38.4 mS/m at 120 g/l.
- Copper powder weight varied with concentration, suggesting the influence of copper ion concentration on deposition efficiency.

3.1.2. Effect of sulfuric acid

Varied sulfuric acid concentrations were employed while keeping other parameters constant. Table 3 presents the conditions and outcomes.

Table 3. Effect of sulfuric acid.

Current (A)	Potential (V)	$CuSO_4$ conc. (g/l)	pH	Time (min)	Electrical conductivity (mS/m)	H_2SO_4 conc. (ml/L)	Copper powder weight (g)
3.0	2.6–4.0	100	0.65–1.52	60	19.21	20	2.36
3.0	2.5–3.8	100	0.52–1.38	60	23.3	30	2.51
3.0	2.4–4.0	100	0.47–1.26	60	34.7	40	2.53
3.0	2.3–3.9	100	0.32–0.91	60	45.5	50	3.31
3.0	2.5–3.9	100	0.21–0.82	60	51.2	60	2.25

Conclusions from Table 3:

- Various sulfuric acid concentrations were explored, maintaining constant copper sulfate concentration;
- Parameters such as current, potential, and pH were consistent, while sulfuric acid concentration increased;
- Electrical conductivity exhibited an upward trend with higher sulfuric acid concentrations.
- Copper powder weight showed variations, emphasizing the impact of sulfuric acid concentration on the deposition process.

3.1.3. Effect of concentration of saliva without incubation

The study introduces 20 g of copper sulfate concentrate to 250 ml of distilled water. Various concentrations (0.25, 0.50, 0.75 and 1 g) of fresh saliva are added without incubation. Table 4 presents the conditions and results, while Figure 3 illustrates the process.

Table 4. Effect of additive saliva camel concentration (without incubation).

$CuSO_4$ (g/l)	Saliva con. (g)	Potential	pH	Time	Current	Electrical conductivity (mS/m)	Copper powder weight (g)
20	0.25	12.7–20	2.5	1 h	3 A	25.1	2.81
20	0.50	–	3	–	–	22.6	2.85
20	0.75	–	–	–	–	23.1	2.85
20	1	–	–	–	–	25.8	2.91

Conclusions from Table 4:

- The study explored the impact of different concentrations of camel saliva without incubation.
- Saliva concentrations ranging from 0.25 g to 1 g were investigated.
- Parameters such as potential, pH, time, current, and electrical conductivity were considered.
- Copper powder weight exhibited variations, indicating the influence of saliva concentration on the deposition process.

Table 5. Activity of saliva.

Sample no.	Saliva activity (U/ml)
1	1.1
2	1.13
3	0.63

Figure 3. (a) Saliva powder, (b) collecting camel saliva.

3.2. Apparent density

To estimate apparent density, the powder was poured into a known-sized empty container. The apparent density (ρ) is calculated using the following equation:

$$\rho = \frac{W_2 - W_1}{V_p}$$

where: W_1 is the weight of the empty vessel (g); W_2 is the weight of the container filled with powder (g); V_p is the powder volume (cm^3); ρ is the apparent density (g/cm^3).

4. Results and Discussion

4.1. Tafel extrapolation method (corrosion behavior of copper deposits)

The corrosion resistance of various copper deposits obtained at 37°C and 3 A from different baths was evaluated using the Tafel extrapolation method. Figure 4 presents electrochemical parameters from corrosion resistance studies, including E_{corr}, i_{corr}, and Tafel slopes [51, 53]. Figure 4a, b illustrates higher corrosion current density and corrosion potential for copper deposits without additives compared to those from additive-containing baths, as shown in Figure 5a, b. The anodic Tafel slope is less active in the presence of additives, resulting in lower corrosion current and corrosion potentials shifting to the noble direction. The weight loss of copper samples immersed in the brine solution without inhibitors showed a significant decrease, indicating anodic dissolution stimulation and adsorption of anti-polarizing ions such as (SO_4^{2-}). In contrast, the weight loss decreased gradually in the presence of inhibitors, suggesting the formation of a protective organic inhibitor layer on the copper surface. The corrosion effort deviates in the positive direction, indicating a more noble and less effective corrosion direction.

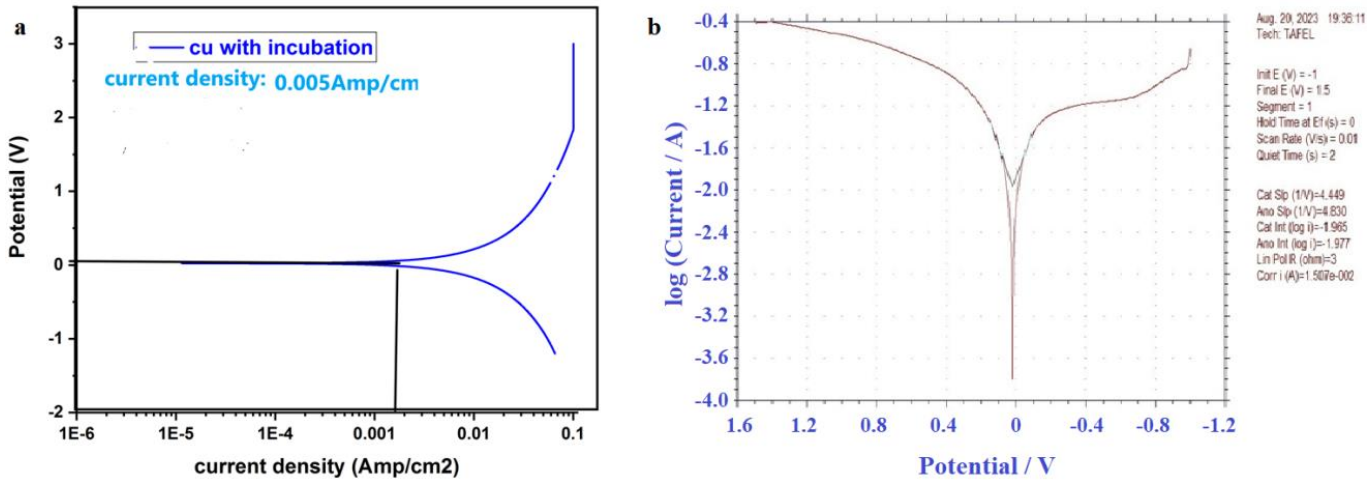

Figure 4 (a, b). Polarization curves for copper without addition under process conditions.

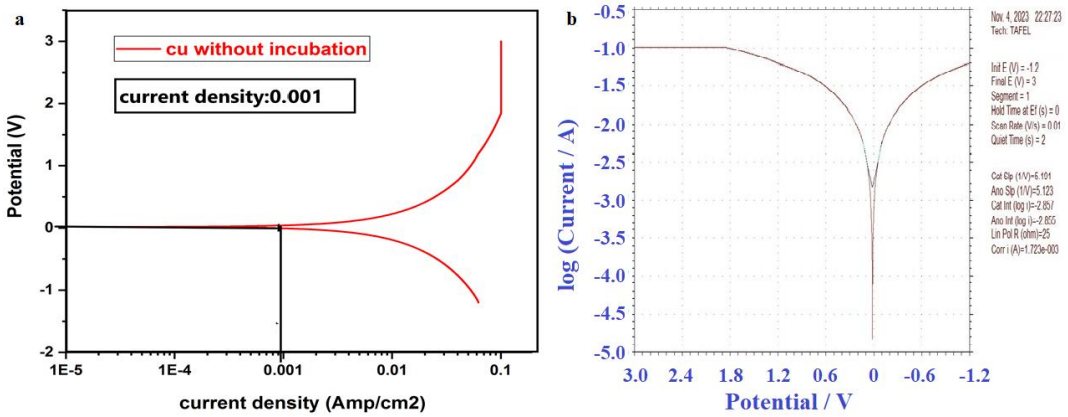

Figure 5 (a, b). Polarization curves of copper with the addition of saliva under process conditions.

4.2. FE-SEM characterization

The effect of $CuSO_4$ solution concentration (40, 60, 80, 100 and 120 g/l) on the mass of copper deposited on the cathode electrode at constant conditions was examined to determine optimal concentrations [54]. Observations revealed a decrease in copper powder weight with increasing copper sulfate concentration, signifying the additive's role in embracing and reducing copper ions while minimizing other impurities, as depicted in Figure 6a, b. The FE-SEM morphology without additive, as presented in Figure 7a, b at 40 and 60 g/L copper concentrations, exhibited relatively small and densely distributed nuclei on the surface. At higher copper concentrations, the nuclei size increased, while the population density decreased, forming a honeycomb-like structure at elevated copper concentrations, as observed in Figure 8a, b. The change in morphology of electrodeposited copper with increasing Cu(II) ions concentration is attributed to the decrease in solution stirring effectiveness due to evolved hydrogen and a decrease in the relative concentration of H^+ ions with increasing Cu concentration. The morphology with the addition of saliva revealed spherical particles with an average size of about 36.5 nm, as shown in Figure 9a, b.

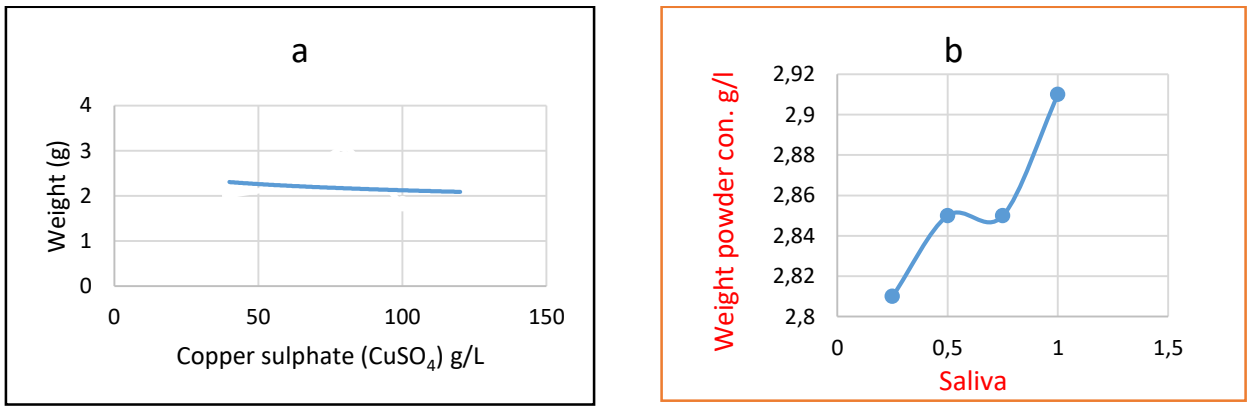

Figure 6. (a) Relationship between copper sulphate and mass product, (b) relationship between saliva and mass product.

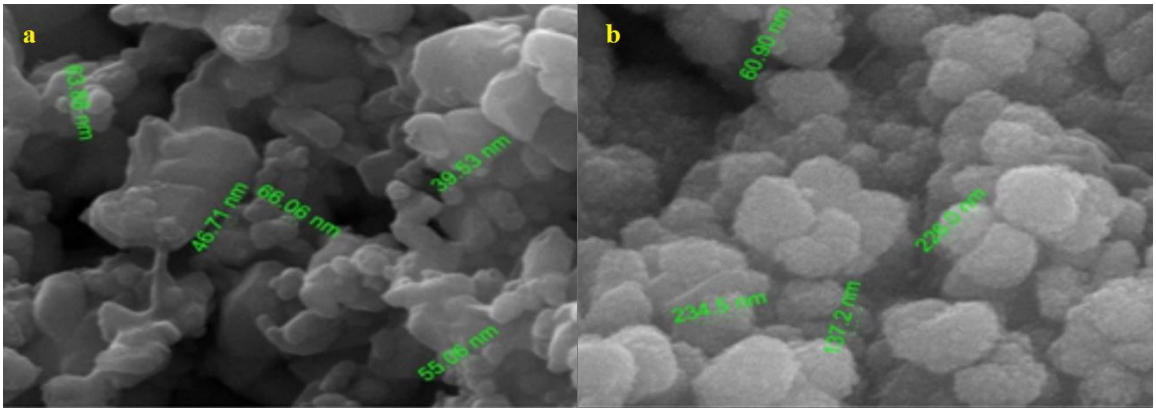

Figure 7 (a, b). Morphology of copper powder at initial concentrations without additive.

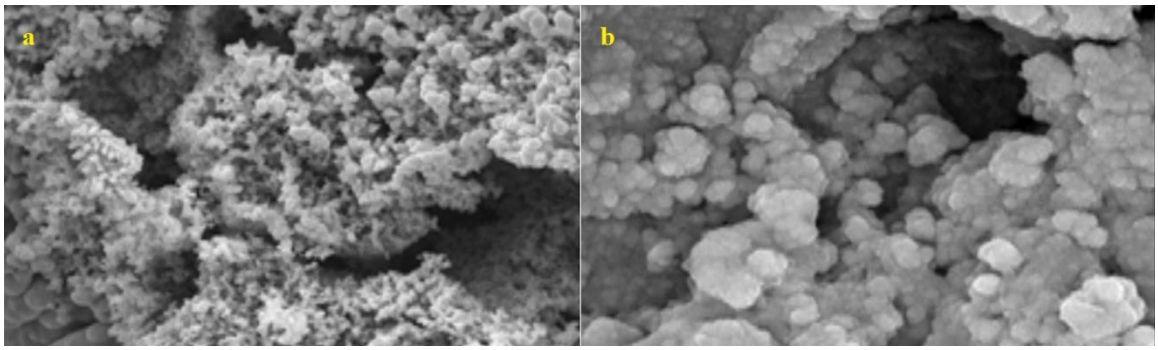

Figure 8 (a, b). Morphology of copper powder at final concentrations without additive.

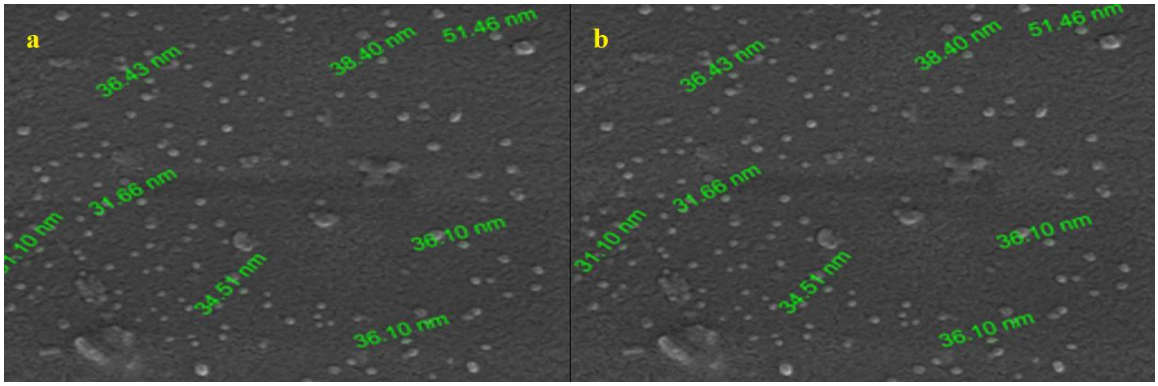

Figure 9 (a, b). Morphology of copper powder with added saliva at different concentration.

In summary, the experimental results indicate the effectiveness of saliva as an additive in controlling the morphology and size of copper deposits during electrodeposition, contributing to enhanced corrosion resistance and surface characteristics.

4.3. EDX spectra

The data obtained from EDX analyses are presented as a plot of energy *vs* intensity. X-rays emitted from each metal are known to have a characteristic identity having the same wavelength and energy with the same position in the EDX, EDX data can also be represented

as atomic weight % of the constituent elements represented by using the best sample obtained and compared to the best samples obtained after addition that show low O concentration in deposit as in Figure 10–12 and Table 6.

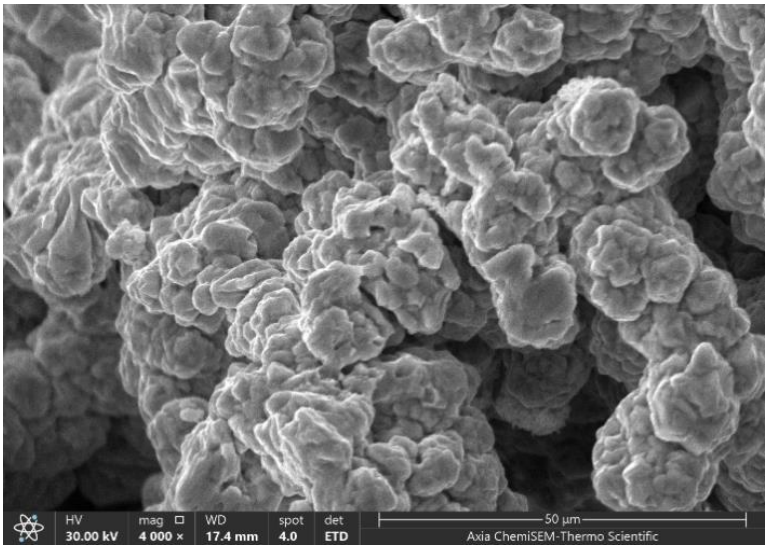

Figure 10. Morphologhy of copper powder before additive saliva.

Table 6. Elemental composition of copper product.

Element	Atomic %	Atomic % error	Weight %	Weight % error
C	36.6	0.9	10.4	0.3
O	4.8	0.5	1.8	0.2
Cu	58.6	0.3	87.8	0.5

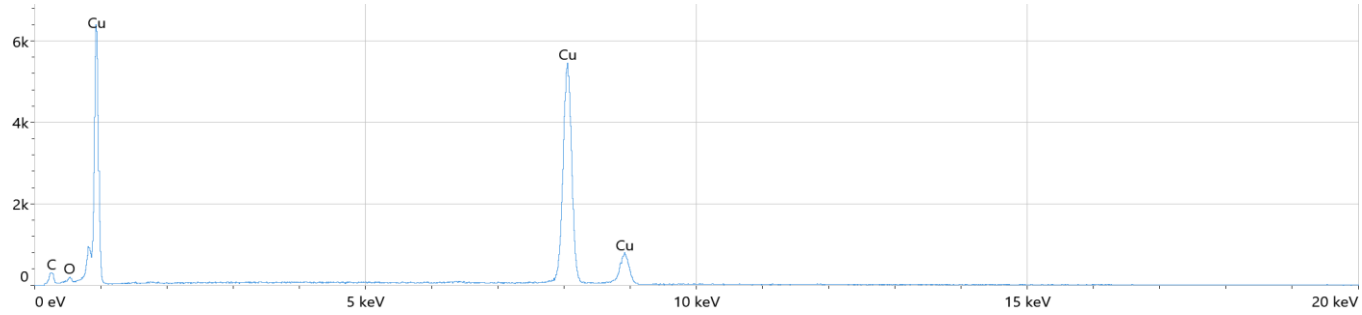

Figure 11. EDX spectrum of the copper powder with 20 g of copper sulphate without additive saliva under one hour, 3 A condition.

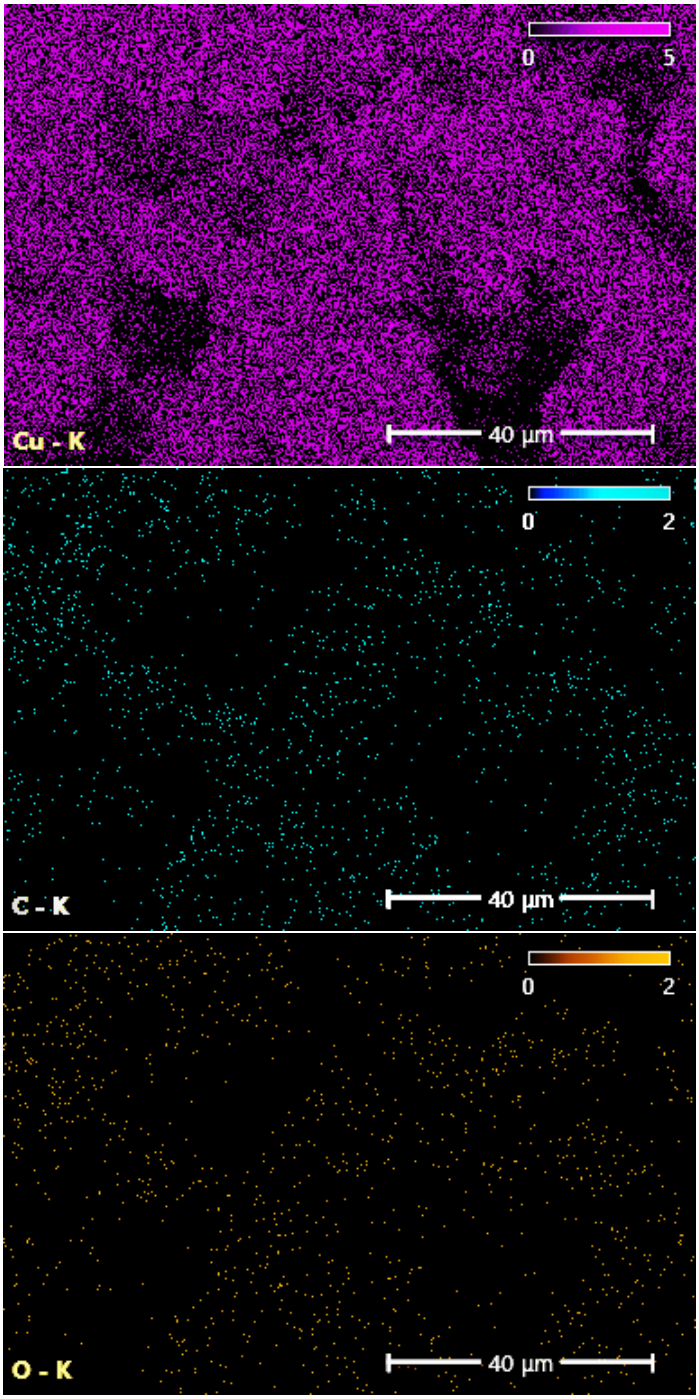

Figure 12. FE-SEM.

The energy-dispersive X-ray (EDX) diagrams obtained from the amino acid – Cu nanoparticles shows high peaks of the copper element and other impurities such as Al, Cl, C, O and it can be noted that the amount of oxygen has become high as a result of the purification of the addition consisting of carboxyl amino acids as in Figures 13, 14 and in Table 7.

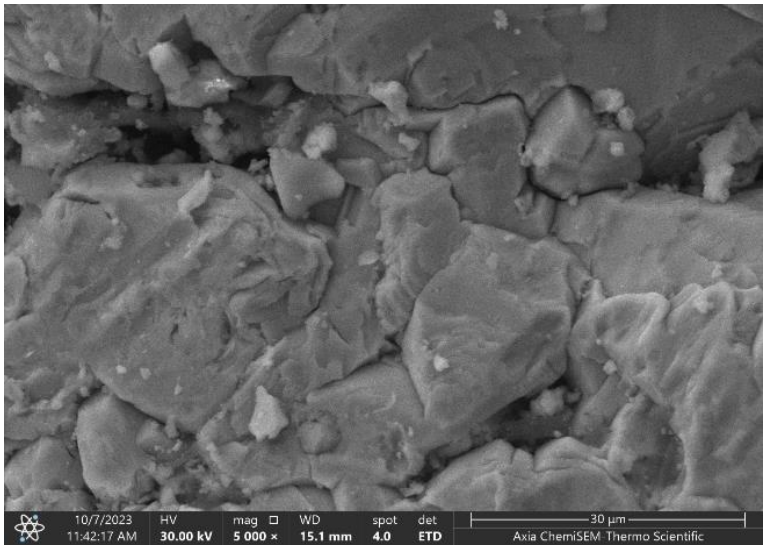

Figure 13. FE-SEM.

Table 7. The elements and atomic percent.

Element	Atomic %	Atomic % error	Weight %	Weight % error
C	38.9	0.9	12.5	0.3
O	12.0	0.4	5.1	0.2
Al	0.3	0.1	0.2	0.1
Si	0.5	0.1	0.4	0.0
Cl	0.2	0.0	0.1	0.0
Cu	48.2	0.3	81.7	0.5

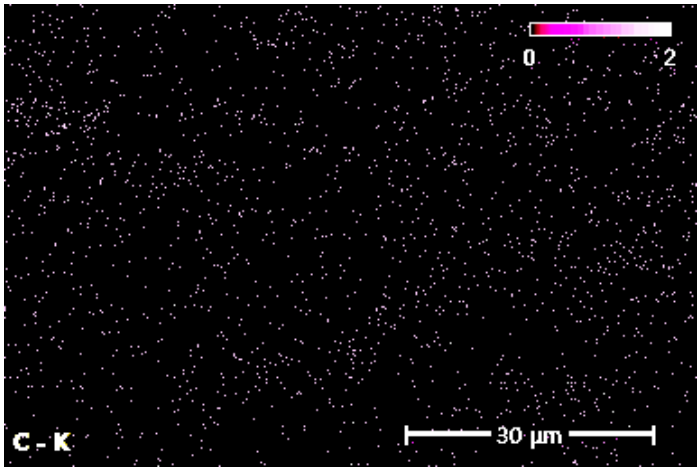

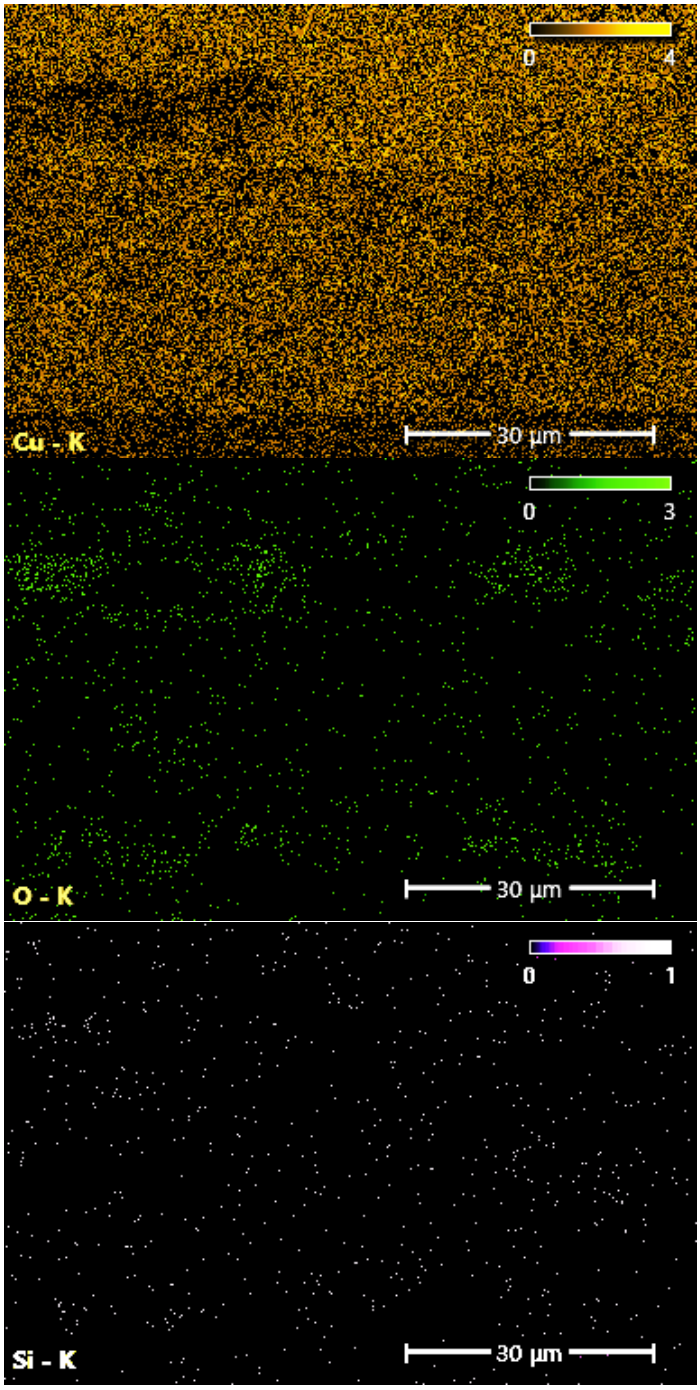
0
4
Cu - K
30 µm
0
3
O - K
30 µm
0
1
Si - K
30 µm

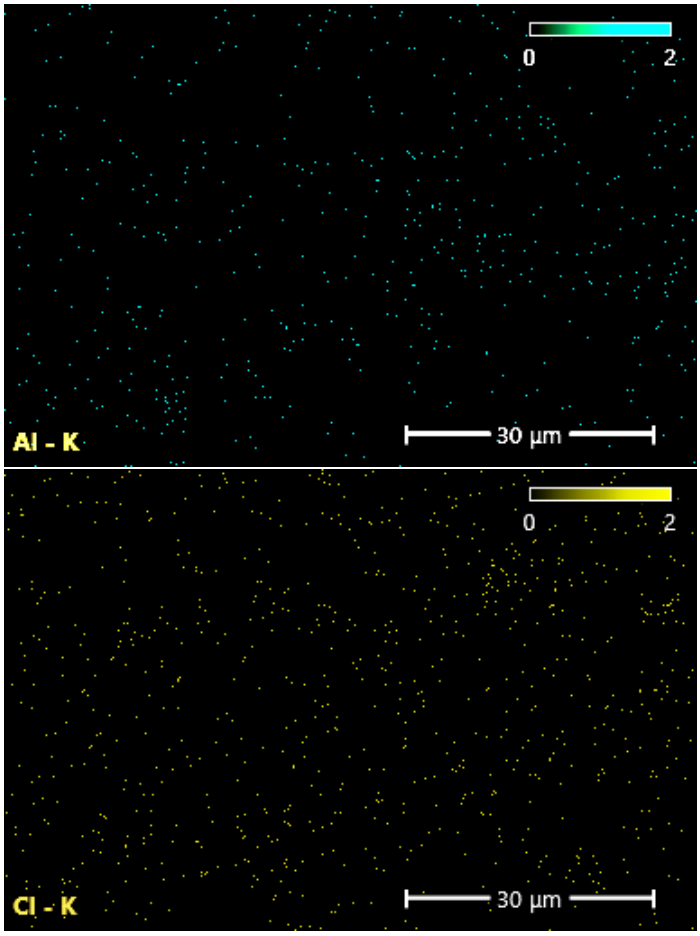

Figure 14. Morphology of copper powder, elemental composition, EDX spectra and FE-SEM image of mechanically scrubbed copper surface.

4.4. DLS measurement

Dynamic light scattering (DLS) analysis allows safely measuring particle dimensions distribution in the sub-micron range [55]. This technique is particularly useful for studying the behavior of nanoparticles in suspensions. The dynamic light Scattering measurement of copper nanoparticles; the average size obtained of the particle size with a narrow size distribution. The size distribution of the particles was determined by DLS and was found to be 85–35 nm. This depends on the concentration of the added saliva, as the higher the concentration, the smaller the granular size.

4.5. FTIR analysis spectrophotometry

Simple test for verification of binding of organic mineral has not been available [56, 57]. There are varieties of tests which make subjective measurement of quality rather than chelation. The only method to verify that the product is an amino acid chelate is to look at the bonds that exist between the metal and the ligand. According to this FTIR technique is more useful to examine the product chelation. The presence of the dopant in the doped crystals was confirmed qualitatively by the FT-IR spectroscopy, FTIR spectrum was

recorded in the range between 4000 cm^{-1} to 500 cm^{-1}. Presence of amino group confirmed due to O–H bond stretch appears as strong broad in carboxylic acid compound, this strong broadband is positioned at the left end of the spectrum, in the range of about 3300 to 2500 cm^{-1} and peak at 2652 cm^{-1}, indicating the formation of CuNPs, these bands appear to be shifted toward lower frequencies in the spectra of the complexes with C–N bond at 749 cm^{-1} between 858–733cm^{-1}.

5. Apparent Density Analysis

By observing Figure 15a, the bulk density increases with increasing copper ion concentration, and compared to Figure 15b, in which natural saliva was added, we notice a higher increase in the bulk density than without the addition because its particles surround themselves with a large layer of the diffusion medium, to which they are closely linked [57–59].

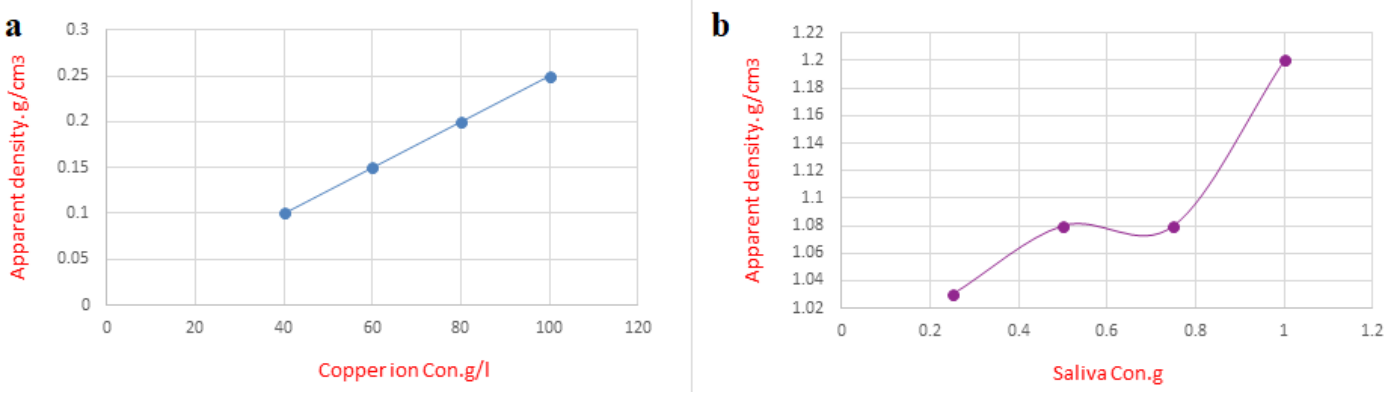

Figure 15. (a) Relationship between concentration apparent density; (b) relationship between saliva concentration and apparent density.

6. Conclusion

In this study, we utilized amino acids derived from saliva extracted from camels in Basra, southern Iraq, as a source for synthesizing copper nanoparticles (CuNPs). The investigated α-amino acids, characterized by a carboxyl group and an amine group in the α-position, exhibited variations in side chain structures, imparting unique physicochemical properties to each amino acid. The synthesis process involved treating saliva with $CuSO_4 \cdot 5H_2O$ at concentrations of 0.25, 0.50, 0.75 and 1 g. The resulting changes in salivary proteins were meticulously analyzed through techniques such as FT-IR spectrophotometry, dynamic light scattering (DLS) analysis, field-emission scanning electron microscopy (FE-SEM), and differential electrical conductivity (DEX). The evaluation of results revealed nanoparticle sizes of approximately 30 nm, showcasing the effectiveness of this approach in tailoring the physicochemical characteristics of copper nanoparticles through the use of camel saliva-derived amino acids. This research contributes valuable insights into the potential applications of environmentally friendly and locally sourced materials for nanomaterial synthesis.

References

1. A.A. Al-Amiery, W.K. Al-Azzawi and W.N.R.W. Isahak, Isatin Schiff base is an effective corrosion inhibitor for mild steel in hydrochloric acid solution: gravimetrical, electrochemical, and computational investigation, *Sci. Rep*., 2022, **12**, 17773. doi: 10.1038/s41598-022-22611-4
2. B.S. Mahdi, M.K. Abbass, M.K. Mohsin, W.K. Al-azzawi, M.M. Hanoon, M.H.H. Al-kaabi, L.M. Shaker, A.A. Al-amiery, W.N.R.W. Isahak, A.A.H. Kadhum and M.S. Takriff, Corrosion inhibition of mild steel in hydrochloric acid environment using terephthaldehyde based on Schiff base: gravimetric, thermodynamic and computational studies, Molecules, 2022, **27**, 4857. doi: 10.3390/molecules27154857
3. A.M. Resen, M. Hanoon, R.D. Salim, A.A. Al-Amiery, L.M. Shaker and A.A.H. Kadhum, Gravimetrical, theoretical, and surface morphological investigations of corrosion inhibition effect of 4-(benzoimidazole-2-yl) pyridine on mild steel in hydrochloric acid, *Koroze Ochr. Mater*., 2020, **64**, 122–130. doi: 10.2478/kom-2020-0018
4. W.K. Al-Azzawi, S.M. Salih, A.F. Hamood, R.K. Al-Azzawi, M.H. Kzar, H.N. Jawoosh, L.M. Shakier, A. Al-Amiery, A.A.H. Kadhum, W.N.R.W. Isahak and M.S. Takriff, Adsorption and theoretical investigations of a Schiff base for corrosion inhibition of mild steel in an acidic environment, *Int. J. Corros. Scale Inhib*., 2022, **11**, no. 3, 1063–1082. doi: 10.17675/2305-6894-2022-11-3-10
5. H.S. Aljibori, A.H. Alwazir, S. Abdulhadi, W.K. Al-Azzawi, A.A.H. Kadhum, L.M. Shaker, A.A. Al-Amiery and H.Sh. Majdi, The use of a Schiff base derivative to inhibit mild steel corrosion in 1 M HCl solution: a comparison of practical and theoretical findings, *Int. J. Corros. Scale Inhib*., 2022, **11**, no. 4, 1435–1455. doi: 10.17675/2305- 6894-2022-11-4-2
6. A.A. Al-Amiery, F.F. Sayyid, A.M. Mustafa, S.I. Ibrahim, M.K. Mohsin, M.M. Hanoon, M.H.H. Al-Kaabi, A.H. Kadhum and W.N.R.W. Isahak, Gravimetric Measurements and Theoretical Calculations of 4-Aminoantipyrine Derivatives as Corrosion Inhibitors for Mild Steel in Hydrochloric Acid Solution: Comparative Studies, *Corros. Sci. Technol*., 2023, **22**, no. 2, 73−89. doi: 10.14773/cst.2023.22.73
7. M.M. Hanoon, A.M. Resen, A.A. Al-Amiery, A.A.H. Kadhum and M.S. Takriff, Theoretical and experimental studies on the corrosion inhibition potentials of 2-((6-methyl-2-ketoquinolin-3-yl) methylene) hydrazinecarbothioamide for mild steel in 1 M HCl, *Prog. Color Colorants Coat*., 2022, **15**, 21–33. doi: 10.30509/PCCC.2020.166739.1095
8. Y.M. Abdulsahib, A.J.M. Eltmimi, S.A. Alhabeeb, M.M. Hanoon, A.A. Al-Amiery, T. Allami and A.A.H. Kadhum, Experimental and theoretical investigations on the inhibition efficiency of *N*-(2,4-dihydroxytolueneylidene)-4-methylpyridin-2-amine for the corrosion of mild steel in hydrochloric acid, *Int. J. Corros. Scale Inhib*., 2021, **10**, no. 3, 885–899. doi: 10.17675/2305-6894-2021-10-3-3

9. A.K. Khudhair, A.M. Mustafa, M.M. Hanoon, A. Al-Amiery, L.M. Shaker, T. Gazz, A.B. Mohamad, A.H. Kadhum and M.S. Takriff, Experimental and theoretical investigation on the corrosion inhibitor potential of *N*-MEH for mild steel in HCl, *Prog. Color, Color. Coat.*, 2022, **15**, 111–122. doi: 10.30509/PCCC.2021.166815.1111
10. N. Souissi and E. Triki, Modelling of phosphate inhibition of copper corrosion in aqueous chloride and sulphate media, *Corros. Sci.*, 2008, **50**, no. 1, 231–241. doi: 10.1016/j.corsci.2007.06.022
11. C. Blanc, S. Gastaud and G. Mankowski, Mechanistic studies of the corrosion of 2024 aluminum alloy in nitrate solutions, *J. Electrochem. Soc.*, 2003, **150**, no. 8. doi: 10.1149/1.1590327
12. M. Scendo, Inhibition of copper corrosion in sodium nitrate solutions with nontoxic inhibitors, *Corros. Sci.*, 2008, **50**, no. 6, 1584–1592. doi: 10.1016/j.corsci.2008.02.015
13. E.A. Skrypnikova, S.A. Kaluzhina and L.E. Agafonova, Inhibition of copper pitting corrosion in alkaline sulphate media by benzotriazole at elevated temperatures, *Int. J. Corros. Scale Inhib.*, 2014, **3**, no. 1, 59–65. doi: 10.17675/2305-6894-2014-3-1-059-065
14. E.A. Skrypnikova and S.A. Kaluzhina, Inhibition of copper local depassivation in alkaline media with oxygen-containing anions, *Int. J. Corros. Scale Inhib.*, 2017, **6**, no. 2, 142–150. doi: 10.17675/2305-6894-2017-6-2-4
15. E.A. Skrypnikova and S.A. Kaluzhina, Effect of hydrodynamic conditions on copper pitting corrosion inhibition in hydrocarbonate-chloride solutions by benzotriazole, *Int. J. Corros. Scale Inhib.*, 2015, **4**, no. 2, 139–145. doi: 10.17675/2305-6894-2015-4-1-139-145
16. A. Frignani, F. Zucchi, G. Trabanelli and C. Monticelli, Alkyl-benzotriazole derivatives as inhibitors of iron and copper corrosion, *Int. J. Corros. Scale Inhib.*, 2015, **4**, no. 1, 96–107. doi: 10.17675/2305-6894-2015-4-1-096-107
17. I.A. Arkhipushkin, L.P. Kazansky, S.S. Vesely and Y.E. Pronin, Electrochemical and XPS study of 2-mercaptobenzothiazole nanolayers on zinc and copper surface, *Int. J. Corros. Scale Inhib.*, 2014, **3**, no. 2, 78–88. doi: 10.17675/2305-6894-2014-3-2-078-088
18. Yu.I. Kuznetsov and L.P. Kazanski, Physicochemical aspects of metal protection by azoles as corrosion inhibitors, *Russ. Chem. Rev.*, 2008, **77**, no. 3, 219–232.
19. K. Cho, J. Kishimoto, T. Hashizume, H.W. Pickering and T. Sakurai, Adsorption and film growth of BTA on clean and oxygen adsorbed Cu (110) surfaces, *Appl. Surf. Sci.*, 1995, 87–88, 380-385.
20. T. Kosec, D.K. Merl and I. Milošev, Impedance and XPS study of benzotriazole films formed on copper, copper–zinc alloys and zinc in chloride solution, *Corros. Sci.*, 2008, **50**, 1987.
21. S. Liu, N. Xu, J. Zeng, Z. Feng and R. Xiao, Corrosion inhibition of carbon steel in tetra-*n*-butylammonium bromide aqueous solution by benzotriazole and Na_3PO_4, *Corros. Sci.*, 2009, **51**, 1356.

22. D. Gallant, M. Pézolet and S. Simard, Inhibition of cobalt active dissolution by benzotriazole in slightly alkaline bicarbonate aqueous media, *Electrochim. Acta*, 2007, **52**, 4927.
23. F. Todt, *Korroziya i zashchita ot korrozii (Corrosion and Corrosion Protection)*, Moscow, Khimiya, 1966, p. 847 (in Russian).
24. N.D. Tomashov and G.P. Chernova, *Passivnost' i zashchita metallov ot korrozii (Passivity and Corrosion Protection of Metals)*, Moscow, Nauka, 1965 (in Russian).
25. G.G. Uhlig, *Korroziya i bor'ba s nei. vvedenie v korrozionnuyu nauku i tehniku (Corrosion and Corrosion Prevention. Introduction to Corrosion Science and Technology)*, Leningrad, Khimiya, 1989 (in Russian).
26. A. Al-Amiery, W.N.R.W. Isahak and W.K. Al-Azzawi, Sustainable corrosion Inhibitors: A key step towards environmentally responsible corrosion control, *Ain Shams Eng. J.*, 2024, 102672. 10.1016/j.asej.2024.102672
27. O.Yu. Grafov, L.P. Kazansky, S.V. Dubinskaya and Yu.I. Kuznetsov, Adsorption of depocolin and inhibition of copper dissolution in aqueous solutions, *Int. J. Corros. Scale Inhib.*, 2019, **8**, no. 3, 549−559. doi: 10.17675/2305-6894-2019-8-3-6
28. V.I. Kolodov, V.V. Trineeva, N.S. Terebova, I.N. Shabanova, T.M. Makhneva, R.V. Mustakimov and A.A. Kopylova, The changes in the electron structure and magnetic characteristics of modified copper/carbon nanocomposites, *Chem. Phys. Mesoscopy*, 2018, **20**, no. 1, 72−79 (in Russian).
29. M. Derrick, J. Galkowski, L. Wang, J. Luo and C. Zhong, Synthesis of size-controlled and shaped copper nanoparticles, *Langmuir*, 2007, **23**, no. 10, 5740–5745.
30. L. Ruihan, W. Hao, L. Kong, K. Zhao, H. Bai and Z. Liu, A simple method for the synthesis of copper nanoparticles from metastable intermediates, *RSC Adv.*, 2023, **13**, no. 21, 14361–14369.
31. B. Galindo, R.P.Y. Reyes-Rodriguez, B.A. Puente-Urbina, C.A. Avila-Orta, O.S. Rodríguez-Fernández, G. Cadenas-Pliego, R.H. Lira-Saldivar and L.A. García-Cerda, Synthesis of copper nanoparticles by thermal decomposition and their antimicrobial properties, *J. Nanomater.*, 2014, **2014**, 1–10.
32. A. Tamilvanan, K. Balamurugan, T. Mohanraj and Y. Admassu, Modeling and optimization of electrodeposition process for copper nanoparticle synthesis using ANN and nature-inspired algorithms, *J. Nanomater.*, 2023, **2023**, 1–8.
33. I. DeAlba-Montero, J. Guajardo-Pacheco, E. Morales-Sánchez, R. Araujo-Martínez, G.M. Loredo-Becerra, G. Martínez-Castañón, F. Ruiz and M.E.C. Jasso, Antimicrobial properties of copper nanoparticles and amino acid chelated copper nanoparticles produced by using a soya extract, *Bioinorg. Chem. Appl.*, 2017, **2017**, 1–11.
34. S.A.M. Al-Bat'hi, Electrodeposition of nanostructure materials, InteChopen, 2015, 2. https://www.Intechopen.Com/Chapters/49413
35. T.P. Moffat, D. Wheeler and D. Josell, Electrodeposition of copper in the SPS-PEG-Cl additive system I. Kinetic Measurements: Influence of SPS, *J. Electrochem. Soc.*, 2004, **151**, no. 4, 262–271. doi: 10.1149/1.1651530

36. K. Kondo, N.R. Akolkar, D.P. Barkey and M. Yokoi, Copper electrodeposition for nanofabrication of electronics devices, *Nanostruct. Sci. Technol*., Springer New York Heidelberg Dordrecht London, 2014, **171**, 282. doi: 10.1007/978-1-4614-9176-7
37. Zh. Li, 1.B. Tan, M. Shi, J. Luo, Zh. Hao, J. He, G. Yang, and Ch. Cui, Bis-(sodium sulfoethyl)-disulfide: A promising agent for superconformal copper electrodeposition with wide operating concentration ranges, *J. Electrochem. Soc*., 2020, **167**, 042508. doi: 10.1149/1945-7111/ab7b85
38. M. Tan and J.N. Harb, Additive Behavior during copper electrodeposition in solutions containing Cl^-, PEG, and SPS, *J. Electrochem. Soc*., 2003, **150**, no. 6, 420–425. doi: 10.1149/1.1570412
39. M.J. Willey, A.C. West, SPS Adsorption and desorption during copper electrodeposition and its impact on PEG adsorption, *J. Electrochem. Soc*., 2003, **154**, no. 3, 156–162. doi: 10.1149/1.2431320
40. J.J. Kelly, Ch. Tian and A.C. West, Leveling and microstructural effects of additives for copper electrodeposition, *J. Electrochem. Soc*., 1999, **146**, no. 7, 2540–2545. doi: 10.1149/1.1391968
41. M.A. Pasquale, L.M. Gassa and A.J. Arvia, Copper electrodeposition from an acidic plating bath containing accelerating and inhibiting organic additives, *Electrochim. Acta*, 2008, **53**, no. 20, 5891–5904. doi: 10.1016/j.electacta.2008.03.073
42. R.T. Rooney, H. Jha, D. Rohde, R. Schmidt and A.A. Gewirth, Suppression of copper electrodeposition by PEG in methanesulfonic acid electrolytes, *J. Electrochem. Soc*., 2019, **166**, no. 13, 551–558. doi: 10.1149/2.0171913jes
43. X. Liang, X. Ren, R. He, T. Ma and A. Liu, Theoretical and experimental study of the influence of PEG and PEI on copper electrodeposition, *New J. Chem*., 2021, **45**, 19655–19659. doi: 10.1039/D1NJ03503G
44. S. Ren, Z. Lei and Z. Wang, Investigation of suppressor polyethylene glycol dodecyl ether on electroplated Cu filling by electrochemical method, *Trans. IMF*, 2015, **93**, no. 4, 190–195. doi: 10.1179/0020296715Z.000000000251
45. Z. Li, B. Tan, M. Shi, J. Luo, Z. Hao, J. He, G. Yang and C. Cui, Bis-(sodium sulfoethyl)-disulfide: A promising agent for superconformal copper electrodeposition with wide operating concentration ranges, *J. Electrochem. Soc*., 2020, **167**, no. 4, 548–559. doi: 10.1149/1945-7111/ab7b85
46. O.Yu. Grafov, L.P. Kazansky, S.V. Dubinskaya and Yu.I. Kuznetsov, Adsorption of depocolin and inhibition of copper dissolution in aqueous solutions, *Int. J. Corros. Scale Inhib*., 2019, **8**, no. 3, 549−559. doi: 10.17675/2305-6894-2019-8-3-6
47. I.N. Shabanova, S.M. Reshetnikov, E.A. Naimushina and N.S. Terebova, XPS investigation of adsorption protective layers based on industrial inhibited oil, *Int. J. Corros. Scale Inhib*., 2020, **9**, no. 2, 903–911. doi: 10.17675/2305-6894-2020-9-3-6
48. Ya.G. Avdeev, D.S. Kuznetsov, M.V. Tyurina and M.A. Chekulaev, Protection of nickel-chromium steel in sulfuric acid solution by a substituted triazole, *Int. J. Corros. Scale Inhib*., 2015, **4**, no. 2, 146−161. doi: 10.17675/2305-6894-2015-4-1-146-161

49. N.A. Gladkikh, M.A. Maleeva, L.B. Maksaeva, M.A. Petrunin, A.A. Rybkina, T.A. Yurasova, A.I. Marshakov and R.Kh. Zalavutdinov, Localized dissolution of carbon steel used for pipelines under constant cathodic polarization conditions. Initial stages of defect formation, *Int. J. Corros. Scale Inhib*., 2018, **7**, no. 4, 683−696. doi: 10.17675/2305-6894-2018-7-4-14
50. I.N. Shabanova, S.M. Reshetnikov, V.I. Kodolov, N.S. Terebova, R.V. Mustakimov, F.F. Chausov and S.G. Bystrov, Investigation of copper/carbon nanocomposites modified with phosphorus-containing groups as inhibiting additives in mineral oil, *Int. J. Corros. Scale Inhib*., 2020, **9**, no. 4, 1381–1389. doi: 10.17675/2305-6894-2020-9-4-11
51. K.F. Khaled and M.M. Al-Qahtani, The inhibitive effect of some tetrazole derivatives towards Al corrosion in acid solution: Chemical, electrochemical and theoretical studies, *Mater. Chem. Phys*., 2009, **113**, 150–158. doi: 10.1016/j.matchemphys.2008.07.060
52. R.F.V. Villamil, P. Corio, J.C. Rubin and S.M.L. Agostinho, Effect of sodium dodecylsulfate on copper corrosion in sulfuric acid media in the absence and presence of benzotriazole, *J. Electroanal. Chem*., 1999, **472**, 112–116. doi: 10.1016/S0022-0728(99)00267-3
53. H. Keles, M. Keles, I. Dehri and O. Serinday, Adsorption and inhibitive properties of aminobiphenyl and its Schiff base on mild steel corrosion in 0.5 M HCl medium, Colloids Surf A, 2008, **320**, 138–145. doi: 10.1016/j.colsurfa.2008.01.040
54. S. Echihi, M. Tabyaoui and W. Qafsaoui, Inhibitive effect of 1,3,4-thiadiazole-2,5-dithiol on copper corrosion in chloride media, *Int. J. Corros. Scale Inhib*., 2019, **8**, no. 2, 329–355. doi: 10.17675/2305-6894-2019-8-2-14
55. K.I. Popov, M.S. Oshchepkov, N.A. Shabanova, Yu.M. Dikareva, V.E. Larchenko and E.Ya. Koltinova, DLS study of a phosphonate induced gypsum scale inhibition mechanism using indifferent nanodispersions as the standards for light scattering intensity comparison, *Int. J. Corros. Scale Inhib*., 2018, **7**, no. 1, 9–24. doi: 10.17675/2305-6894-2018-7-1-2
56. M.A. Ayyash, M.J. Ewadh and N.J. Mohammed, Qualitative and quantitative determination of anti-cancer drug (vincristine) in catharanthus roseus by high performance liquid chromatography and qualitative identification using other molecular spectra instruments, *Res. J. Pharm., Biol. Chem. Sci*., 2016, **7**, no. 4, 1903.
57. W.M.K.W.M. Ikhmal, M.Y.N. Yasmin, M.F.F. Maria, S.M. Syaizwadi, W.A.W. Rafizah, M.G.M. Sabri and B.M. Zahid, Evaluating the performance of Andrographis paniculata leaves extract as additive for corrosion protection of stainless steel 316L in seawater, *Int. J. Corros. Scale Inhib*., 2020, **9**, no. 1, 118–133. doi: 10.17675/2305-6894-2020-9-1-7
58. A.N. Serov, V.S. Makhina, T.A. Vagramyan, V.E. Kasatkin and N.A. Asnis, The possible use of tin ion discharge inhibition in bronze electroplating from an electrolyte based on nitrilotrimethylphosphonic acid, *Int. J. Corros. Scale Inhib*., 2022, **11**, no. 2, 594–605. doi: 10.17675/2305-6894-2022-11-2-9

59. V. Deluchat, J.C. Bollinger, B. Serpaud and C. Caullet, Divalent cations speciation with three phosphonate ligands in the pH-range of natural waters, *Talanta*, 1996, **44**, no. 5, 897–907. doi: 10.1016/s0039-9140(96)02136-4

♦ ♦ ♦